Nanoscale

PAPER

View Article Online
View Journal | View Issue

Cite this: *Nanoscale*, 2018, **10**, 17699

Highly efficient and stable semi-transparent perovskite solar modules with a trilayer anode electrode†

Kun-Mu Lee,*[a,b,c] Kai-Shiang Chen,[a] Jia-Ren Wu,[d] Yan-Duo Lin,*[e] Sheng-Min Yu[f] and Sheng Hsiung Chang *[d]

Received 29th July 2018,
Accepted 3rd September 2018

DOI: 10.1039/c8nr06095a

rsc.li/nanoscale

Highly efficient and stable semi-transparent $CH_3NH_3PbI_3$ perovskite photovoltaic cells are realized by using an ITO/MoO_x bilayer conductive oxide as the anode electrode with a cyclopenta[2,1-*b*;3,4-*b*′]dithiophene (CT) based hole-transport material (HTM), which allows bifacial illumination from both sides of the electrodes. The wide bandgap MoO_x thin film is not only to be an electron blocking layer, but also to be a passivation layer which can withstand the excessive energy bombardment during the magnetron sputtering process for the deposition of a high-quality ITO thin film. Atomic-force microscopy images, transmittance spectra and water-droplet contact angle images show that the interfacial contact between MoO_x and hole transport layer (HTL) strongly influences the short-circuit current density (J_{SC}) and fill factor (FF). The highest power conversion efficiency (PCE) values for the bifacial perovskite solar cells (0.16 cm^2) and modules (11.7 cm^2) are 16.38% and 14.96%, respectively. In addition, the PCE of the ITO/MoO_x/CT-HTM based perovskite solar module decreases slowly toward a stable value (~11%) for more than 700 h under wet environment conditions (70 ± 5 RH%).

Introduction

Regular-type tri-halide organic–inorganic perovskite solar cells (Au/spiro-OMeTAD/perovskite/TiO_2/FTO/glass) have reached the desired power conversion efficiency of over 20% (ref. 1–4) for commercial applications. The excellent photovoltaic performance of perovskite solar cells relies on superior optoelectronic characteristics, such as moderate refractive index, large light absorption coefficient, small exciton binding energy, high carrier mobility and long carrier diffusion length.[5–10] In recent years, the thermal stabilities of organic–inorganic perovskite materials have been improved by doping inorganic cations (Rb and/or Cs)[11–13] while retaining the PCE. Li-Doped spiro-OMeTAD materials have been widely used as an efficient hole-transport layer (HTL) in regular-type perovskite based solar cells. However, spiro-OMeTAD materials can be degraded due to the diffused I^- and $CH_3NH_3^+$ ions, which prevents the oxidation of spiro-OMeTAD, thereby decreasing the electrical properties of spiro-OMeTAD materials.[14] A lot of organic hole-transport materials (HTMs) have been developed to be an alternative HTL in order to improve the device stabilities.[15–18] It can be found that Au has to be used as the top electrode for realizing excellent and stable photovoltaic performance. To reduce the fabrication cost, Ag is also widely used as the top electrode in perovskite solar cells. However, the fabrication conditions of Ag electrodes can strongly influence the short-circuit current density (J_{SC}) and fill factor (FF).[19] In general, the Ag electrode has to be thermally deposited on top of an organic electron-transport layer (ETL) or an organic HTL in order to avoid the formation of the Ag/perovksite interface. However, high-quality transparent metal oxide electrodes (ITO and Al-doped ZnO) have to be fabricated by using sputtering methods. It can be predicted that the excessive energy bombardment during the sputtering process for the deposition of a transparent top electrode must damage the ETL or HTL, which results in the formation of recombination centers embedded in the ETL or HTL. In this study, the main goal is to realize highly efficient and stable semi-trans-

[a]*Department of Chemical and Materials Engineering, Chang Gung University, Taoyuan 33302, Taiwan, Republic of China. E-mail: kmlee@mail.cgu.edu.tw*
[b]*Division of Neonatology, Department of Pediatrics, Chang Gung Memorial Hospital, Linkou, Taoyuan 33305, Taiwan, Republic of China*
[c]*Center for Reliability Sciences and Technologies, Chang Gung University, Taoyuan 33302, Taiwan, Republic of China*
[d]*Department of Physics, Chung Yuan Christian University, Taoyuan 32023, Taiwan, Republic of China. E-mail: shchang@cycu.edu.tw*
[e]*Department of Applied Chemistry, National Chiayi University, Chiayi 60004, Taiwan, Republic of China. E-mail: ydlin@mail.ncyu.edu.tw*
[f]*Material and Chemical Research Laboratory, Industrial Technology Research Institute, Hsinchu 31040, Taiwan, Republic of China*
†Electronic supplementary information (ESI) available. See DOI: 10.1039/c8nr06095a

parent perovskite solar cells and modules by using an ITO/MoO_x/HTL trilayer as the top electrode. In addition, the roles and collocation of the MoO_x interlayer were investigated by using atomic-force microscopy images, transmittance spectra and water-droplet contact angle images.

Experiments

A 30 nm thick TiO_2 compact layer was deposited on top of the FTO/glass substrate by spraying a solution of titanium diisopropoxide bis(acetylacetonate) (75 wt% of $Ti(acac)_2OiPr_2$ in isopropanol) at 450 °C. A 200 nm thick mesoporous TiO_2 thin film, which has an average particle size of 20 nm, was printed on top of the compact-TiO_2/FTO/glass substrate using a home-made paste and heated to 500 °C for 30 min. After cooling down to room temperature, the samples were transferred to a nitrogen-filled glove box (<1% RH). The perovskite precursor, which consists of PbI_2 (1.65 M) and CH_3NH_3I (1.65 M) in DMSO and γ-butyrolactone (GBL) (5/5, v/v), was spin-coated on top of the *meso*-TiO_2/compact-TiO_2/FTO/glass substrate with a washing-enhanced nucleation (WEN) process.[20–24] Spiro-OMeTAD or CT based organic molecule was dissolved in chlorobenzene (CB) (50 mg mL^{-1}), and 17.5 μL of a solution of lithium bis(trifluoromethane)sulfonimide (Li-TFSI, 520 mg) in acetonitrile (1 mL) and 28.5 μL of 4-*tert*-butylpyridine (TBP) were added to the HTM/CB solution. Then, the solutions were stirred and heated to 80 °C for 20 min. The HTM/CB solution was spin-coated on top of the perovskite/*meso*-TiO_2/compact-TiO_2/FTO/glass substrate at 2000 rpm for 30 s. The synthesis, optical properties and electrochemical properties of the CT based HTM are listed in the ESI (Fig. S1–S4†). A MoO_x thin film was deposited on top of the HTL/perovskite/*meso*-TiO_2/compact-TiO_2/FTO/glass substrate by using the thermal evaporation method. Finally, a transparent 350 nm thick ITO film was deposited as the top electrode by using the radio-frequency magnetron sputtering method. For comparison, a 100 nm thick Ag film was also deposited by the thermal evaporation method as the top electrode. The active areas of cells and modules (five cells in series on the 5 cm × 5 cm substrate) were fixed at 0.16 cm^2 and 11.7 cm^2, respectively. The schematic of the perovskite solar module is shown in the ESI (Fig. S5†).

An AM 1.5G solar simulator (Yamashita Denso Corporation, YSS-50A, class AAA) was used as the irradiation light source for the current density–voltage (*J–V*) measurements. An illumination intensity of 100 mW cm^{-2} was calibrated before testing. The *J–V* characteristics of the cell under illumination of AM 1.5G simulated sunlight were obtained by applying the external potential bias to the cell and measuring the photocurrent output with a Keithley model 2400 digital source meter (Keithley, USA). An incident photon conversion efficiency (IPCE) spectrometer (EQE-R-3011, ENLI Technology Co. Ltd, Taiwan) calibrated with a single-crystalline silicon reference cell was used for IPCE measurements.

The surface morphologies of the samples were determined by using a tapping-mode atomic-force microscope (Nano-Scope NS3A system, Digital Instrument). The transmittance spectra of the samples were recorded by using a broadband spectrometer (U-4100, Hitachi). The surface wetting properties of the samples were measured by using a contact angle imaging system (JJA-100-S, Jia Yu Apparatus Co. Ltd, Taiwan).

Results and discussion

HTM plays an important role in long-term stability and device performance.[25] Various HTMs have been used as an alternative HTL for realizing highly efficient and stable regular-type perovskite solar cells.[16] Herein we incorporate an electron-rich CT unit as the core in conjunction with hexoxyl substituted triphenylamine end-caps to construct a novel HTM (Fig. S1†). In order to avoid the formation of AgI at the Ag/perovskite interface, a thermally evaporated MoO_x thin film is used as the interlayer between Ag and CT based HTL. The averaged photovoltaic performance from 8 solar cells is listed in Table 1. The J_{SC} (FF) increases from 19.26 mA cm^{-2} (67.5%) to 21.50 mA cm^{-2} (74.1%) with an increase in the thickness of the MoO_x thin film from 0 nm to 15 nm, which can be explained as due to the increased coverage of MoO_x thin films on the HTL. When the thickness of MoO_x thin films increases from 15 nm to 20 nm, the FF moderately decreases from 74.1% to 69.8%, which results in a decrease in the PCE from 16.54% to 15.76%. Therefore, the optimal thickness of the MoO_x thin film as an interlayer in the regular-type perovskite solar cells is 15 nm. It is noted that the valence band minimum of thermally evaporated MoO_x thin films[26] is close to the highest occupied molecular orbital of the CT-based HTL (see Fig. S4†). Therefore, the use of a MoO_x interlayer does not significantly influence the V_{OC} of perovskite solar cells (see Table 1).

A 15 nm thick MoO_x interlayer is sufficient to avoid the formation of the Ag/HTL interface, which results in a highly aver-

Table 1 Photovoltaic performance of the CT based perovskite solar cells with various thicknesses of MoO_x thin films under 1 sun illumination (AM 1.5G, 100 mW cm^{-2}). Ag thin film is used as the top electrode

Thickness of MoO_x (nm)	V_{OC} (V)	J_{SC} (mA cm^{-2})	FF (%)	PCE (%)
0	1.002 ± 0.020	19.26 ± 0.37	67.5 ± 1.4	13.03 ± 0.25
5	1.010 ± 0.020	21.11 ± 0.41	70.6 ± 1.4	15.06 ± 0.29
10	1.008 ± 0.020	21.27 ± 0.43	72.9 ± 1.5	15.63 ± 0.30
15	1.038 ± 0.021	21.50 ± 0.42	75.5 ± 1.5	16.85 ± 0.32
20	1.025 ± 0.021	22.02 ± 0.43	69.8 ± 1.4	15.76 ± 0.31

aged PCE of 16.85%. During device characterization, the PCE of the perovskite solar cells with a 15 nm thick MoO_x interlayer can retain the initial photovoltaic performance for several hours without encapsulation. It means that the MoO_x thin film can effectively resist the diffusion of Ag into the HTL during electrical measurements. It also suggests that the MoO_x interlayer can resist the excessive energy bombardment during the deposition of the top electrode. To realize semi-transparent perovskite solar cells, an ITO thin film is used as the top electrode. Fig. 1 presents the *J–V* curves of the perovskite solar cells fabricated with different top electrodes (Ag or ITO) under illumination from the FTO side and ITO side. The photovoltaic performance of the perovskite solar cells with different HTLs and top electrodes is listed in Table 2. An excellent PCE of 18.10% can be achieved when Ag and spiro-OMeTAD are used as the top electrode and HTL, respectively. It means that the high-quality $CH_3NH_3PbI_3$ perovskite thin film can be fabricated on top of the *meso*-TiO_2 thin film by using the one-step spin-coating method with a WEN process. The PCE decreases from 18.10% to 15.84% when spiro-OMeTAD is replaced with CT as the HTL, which is mainly due to the reduction in the V_{OC} (FF) from 1.074 V (73.9%) to 0.980 (73.1%). The reductions in the V_{OC} and FF mean that the hole mobility and filming property of the spiro-OMeTAD film are better than those of the CT film. However, the use of a 15 nm thick MoO_x interlayer decreases (increases) the PCE when spiro-OMeTAD (CT) is used as the HTL, which is related to the contact at the MoO_x/HTL interface. When the ITO/MoO_x bilayer is used as the top electrode, the PCE of the CT based perovskite solar cells is higher than that of the spiro-OMeTAD based perovskite solar cells. Therefore, the ITO/MoO_x/CT trilayer is an appropriate candidate for the extraction of holes in the bifacial regular-type perovskite solar cells. A high PCE of 16.38% can be realized in the CT based bifacial perovskite solar cells when illuminated from the FTO side. And, the PCE of the bifacial perovskite solar cells decreases from 16.38% (15.54%) to 14.72% (13.84%) when illuminated from the ITO side, which can be explained as due to the partial incident light (wavelength of 400 to 500 nm) being absorbed by the hole transport layer. This was confirmed from the transmittance spectra (Fig. 6) and IPCE data (Fig. S7†).

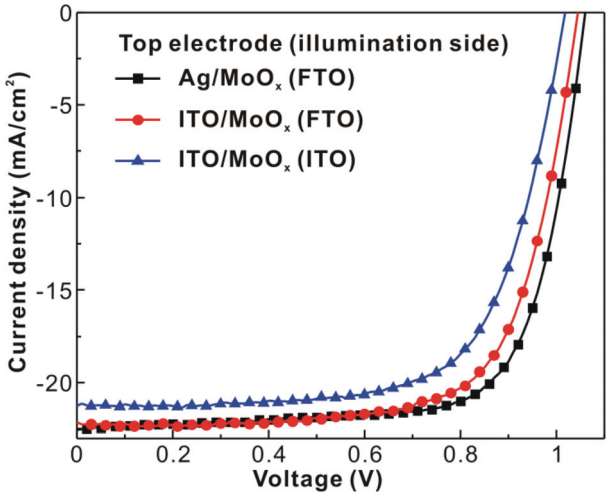

Fig. 1 *J–V* curves of the CT based perovskite solar cells fabricated with different top electrodes under one sun illumination (100 mW cm^{-2}) from the FTO side or ITO side.

To demonstrate that the bifacial perovskite photovoltaic device has the potential in commercial applications, the perovskite module with five cells in a series configuration is fabricated on a 5 cm × 5 cm FTO glass substrate, as shown in Fig. 2. The module with the ITO electrode has a semi-transparent appearance, but that with the Ag electrode is opaque. Fig. 3 presents the *J–V* curves of the CT based perovskite solar modules with different top electrodes. The photovoltaic performance of the perovskite solar modules with different top electrodes is listed in Table 3. The PCE of the CT based perovskite photovoltaic device slightly decreases from 17.25% to 16.43% when the active area increases from 0.16 cm^2 to 11.7 cm^2, which indicates that the $CH_3NH_3PbI_3$, CT and MoO_x thin films can be uniformly fabricated on a large-scale substrate. Moreover, the PCE of the bifacial perovskite photovoltaic device under 1 sun illumination from the FTO side (ITO side) is moderately reduced from 16.38% (14.72%) to 14.96% (13.61%) when the active area increases from 0.16 cm^2 to 11.7 cm^2, which is probably related to the uniformity of the preparation of each layer in this solar module.

Table 2 Photovoltaic performance of the perovskite solar cells with different top electrodes under one sun illumination (AM 1.5G, 100 mW cm^{-2})

Top electrode	HTL	Illumination side	V_{OC} (V)	J_{SC} (mA cm^{-2})	FF (%)	PCE (%)
Ag	Spiro	FTO	1.074	22.80	73.9	18.10
Ag/MoO_x	Spiro	FTO	1.055	22.23	70.7	16.58
Ag	CT	FTO	0.980	22.11	73.1	15.84
Ag/MoO_x	CT	FTO	1.060	22.57	72.1	17.25
ITO/MoO_x	CT	FTO	1.050	22.14	71.0	16.38
ITO/MoO_x	CT	ITO	1.020	21.23	68.3	14.72
ITO/MoO_x	Spiro	FTO	1.025	22.50	67.1	15.54
ITO/MoO_x	Spiro	ITO	1.020	21.82	62.2	13.84

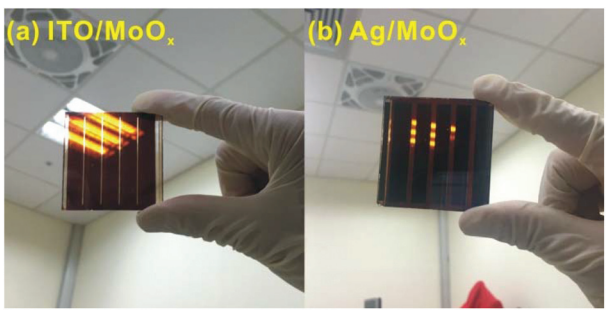

Fig. 2 Photos of the regular-type perovskite solar modules with the CT based hole-transport layer. (a) Top electrode: ITO/MoO_x; (b) top electrode: Ag/MoO_x.

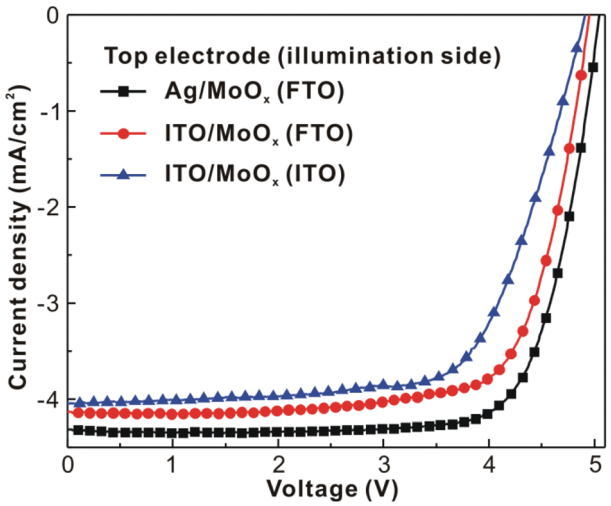

Fig. 3 Photovoltaic performance of the perovskite solar modules (5 cm × 5 cm) with different top electrodes and illumination sides under one sun illumination (AM 1.5G, 100 mW cm^{-2}).

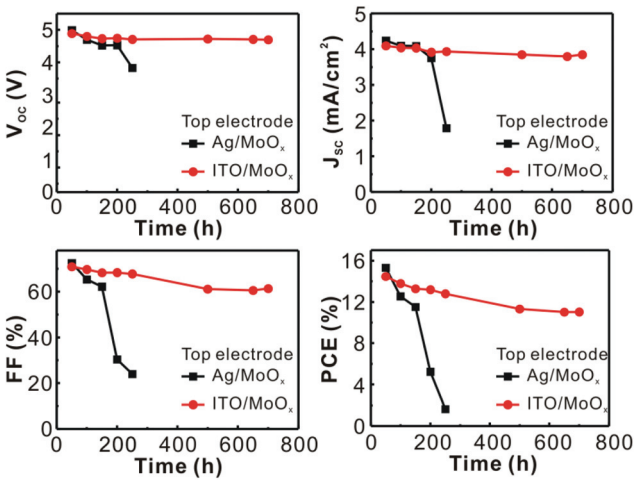

Fig. 4 Time-dependent photovoltaic performance of the CT based perovskite solar modules under a wet environment (26 °C ± 2 °C, 70 ± 5 RH%).

Table 3 Photovoltaic performance of the perovskite solar cells with different top electrodes under one sun illumination (AM 1.5G, 100 mW cm^{-2})

Top electrode	HTL	Illumination side	V_{OC} (V)	J_{SC} (mA cm^{-2})	FF (%)	PCE (%)
Ag/MoO_x	CT	FTO	5.05	4.31	75.5	16.43
ITO/MoO_x	CT	FTO	4.95	4.13	73.2	14.96
ITO/MoO_x	CT	ITO	4.92	4.05	68.3	13.61

To evaluate the device stabilities, the CT based perovskite solar modules were illuminated under a wet environment (26 ± 2 °C, 70 ± 5 RH%) for more than 700 hours. Before the long-term stability test, the experiment of maximum power point tracking (Fig. S8†) was performed. The maximum PCE of the ITO/MoO_x/CT based perovskite solar module is 15.15%, which confirms the high-efficiency photovoltaic device. Fig. 4 presents the time-dependent photovoltaic performance. When the Ag/MoO_x bilayer is used as the top electrode, the PCE decreases gradually toward zero within 250 hours. The decaying curve (black dotted line) exhibits two decay rates which can be explained as due to the diffusion time of Ag into the HTL and reaction with $CH_3NH_3PbI_3$. It means that the MoO_x interlayer cannot effectively block the diffusion of Ag into the HTL. Before the diffused Ag reaches the HTL/perovskite interface (exposure time <150 h), the FF is inversely proportional to the recombination centers (Ag nanoparticles) embedded in the HTL.[19] When the exposure time is larger than 150 hours, the accumulated Ag nanoparticles at the HTL/perovskite interface can generate AgI and simultaneously trap the electrons and holes,[27] and the contact line between the electrodes becomes yellow, which forms the AgI lines (as shown in Fig. S6†), thereby strongly degrading the photovoltaic performance. When the ITO/MoO_x bilayer is used as the top electrode, the photovoltaic performance decreases slowly toward a stable PCE of ~11%. The decaying curve (red dotted line) exhibits a slow decay rate, which can be explained as due to the formation of the surface passivation (PbI_2) at the perovskite grain boundaries.[28] It also means that the MoO_x interlayer can effectively avoid the formation of recombination centers (ITO nanoparticles) in the HTL and the MoO_x/ITO bilayer structure can effectively minimize the moisture-induced degradation on the photovoltaic performance.

The 15 nm thick MoO_x interlayer can effectively passivate the CT during the deposition of the Ag thin film or ITO thin film, thereby increasing the photovoltaic performance. However, the use of a 15 nm thick MoO_x interlayer degrades the PCE of the spiro-OMeTAD based perovskite solar cells from 18.10% to 16.58%. The AFM images, transmittance spectra, and water-droplet contact angle images were used in order to understand the contacts at the MoO_x/CT and MoO_x/spiro-OMETAD interfaces. Fig. 5 presents the AFM images of the CT/perovskite/FTO/glass, MoO_x/CT/perovskite/FTO/glass, spiro-OMeTAD/perovskite/FTO/glass, and MoO_x/spiro-OMeTAD/perovskite/FTO/glass samples. The surface roughness of the MoO_x/CT/perovskite/FTO/glass sample is smaller than that of the CT/perovskite/FTO/glass sample, which means that the 15 nm thick MoO_x can effectively fill the nanometer-scale grooves of the CT thin film. However, the use of a 15 nm thick MoO_x interlayer does not reduce the surface roughness of the spiro-OMeTAD/perovskite/FTO/glass sample, which means that the surface of the spiro-OMeTAD thin film is not completely covered by the MoO_x thin film. Fig. 6 presents the transmittance spectra of the spiro-OMeTAD/FTO/glass, spiro-OMeTAD/MoO_x/FTO/glass, CT/FTO/glass, and MoO_x/CT/ITO/glass samples. The amplitude of the interference ripples in the transmittance spectrum (black line) is reduced by covering the spiro-OMeTAD/FTO/glass sample with a 15 nm thick MoO_x thin film. The reduction in the ripple's amplitude is not

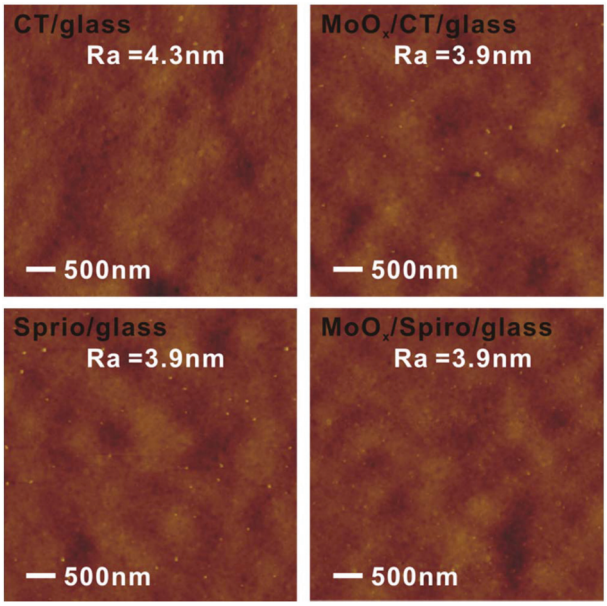

Fig. 5 Atomic-force microscopy images of CT, MoO_x/CT, spiro-OMeTAD and MoO_x/spiro-OMeTAD on perovskite/FTO glass. R_a: arithmetical mean deviation.

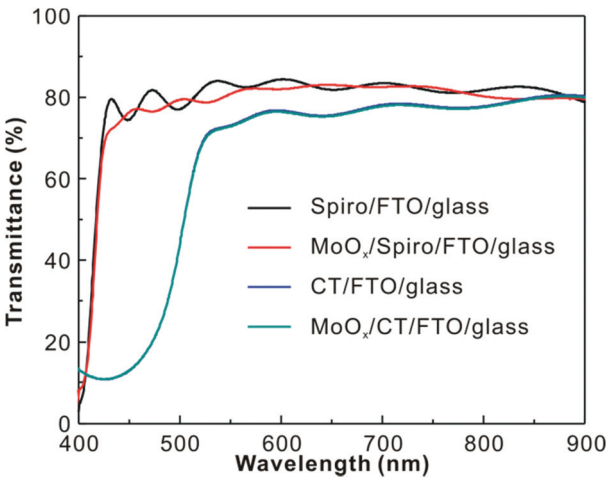

Fig. 6 Transmittance spectra of CT, MoO_x/CT, spiro-OMeTAD and MoO_x/spiro-OMeTAD layers on FTO glass.

related to the light absorption from the capping layer because MoO_x is a wide bandgap material. Therefore, it can be attributed to the increase in the refractive index of the roughened surface from 1.63 (spiro-OMeTAD) to 2.11 (MoO_x) which scatters the incident light and thereby results in a lower amplitude of the interference ripples (red line in Fig. 6). It means that the contact at the MoO_x/spiro-OMeTAD interface is not smooth. However, it is surprising that the capping layer does not influence the transmittance spectrum of the CT/FTO/glass sample, which indicates the formation of a smooth contact at the MoO_x/CT interface. In order to explore the interfacial contact between MoO_x and HTL (spiro-OMeTAD or CT), the surface

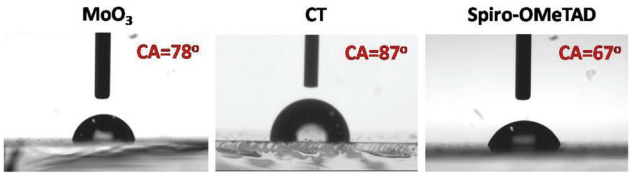

Fig. 7 Water-droplet contact angle (CA) images of MoO_x, CT, and spiro-OMeTAD layers.

wetting properties of the MoO_x, spiro-OMeTAD, and CT thin films were examined as shown in Fig. 7. The spiro-OMeTAD (CT) thin film exhibits a partial wetting (moderate wetting) behavior, which reflects the intrinsic nature of the corresponding molecular structures. The MoO_x thin film exhibits a moderate wetting behavior which indicates a low oxygen defect density.[29] Therefore, the formation of a dense and smooth contact at the MoO_x/CT interface is due to the similar surface properties, which can minimize the formation of recombination centers (Ag nanoparticles or ITO nanoparticles) embedded in the CT thin film. In addition, the contact situation at the MoO_x/HTL interface can be evaluated by using the AFM images in combination with the transmittance spectra and water-droplet contact angle images.

Conclusions

In summary, we have fabricated highly efficient bifacial perovskite solar cells and modules with a stable ITO/MoO_x/CT trilayer anode electrode. The use of a 15 nm thick MoO_x interlayer can effectively resist the excessive energy bombardment during the deposition of the sputtered ITO thin film, which originates from the smooth contact at the MoO_x/CT interface. The ITO/MoO_x/CT based perovskite solar modules exhibited a stable photovoltaic performance under a wet environment, which indicates that the hydrophobic ITO/MoO_x/CT trilayer can effectively minimize the moisture and oxygen induced degradation of the $CH_3NH_3PbI_3$ perovskite thin film.

Conflicts of interest

There are no conflicts to declare.

Acknowledgements

Financial support for this work provided by the Ministry of Science and Technology (MOST) (MOST 106-2731-M-033-002, 106-2218-E-182-005-MY2 and 107-2122-M-033-001-MY3) and the Chang Gung Memorial Hospital, Linkou, Taiwan (CMEPD2G0303 and BMRPC074) is gratefully acknowledged.

References

1 W. S. Yang, J. H. Noh, N. J. Jeon, Y. C. Kim, S. Kim, J. Seo and S. I. Seok, *Science*, 2015, **348**, 1234–1237.
2 M. Saliba, T. Matsui, J.-Y. Seo, K. Domanski, J.-P. Correa-Baena, M. K. Nazeeruddin, S. M. Zakeeruddin, W. T. Tree, A. Abate, A. Hagfeldt and M. Grätzel, *Energy Environ. Sci.*, 2016, **9**, 1989–1997.
3 M. Saliba, T. Matsui, K. Domanski, J.-Y. Seo, A. Ummadisingu, S. M. Zakeeruddin, J.-P. Correa-Baena, W. T. Tree, A. Abate, A. Hagfeldt and M. Grätzel, *Science*, 2016, **354**, 206–209.
4 H. Tan, A. Jain, O. Voznyy, X. Lan, F. P. G. de Arquer, J. Z. Fan, R. Quintero-Bermudez, M. Yuan, B. Zhang, Y. Zhao, F. Fan, P. Li, L. N. Quan, Y. Zhao, Z.-H. Lu, Z. Yang, S. Hoogland and E. H. Sargent, *Science*, DOI: 10.1126/science.aai9081.
5 S. H. Chang, K.-F. Lin, C.-H. Chiang, S.-H. Chen and C.-G. Wu, *Sci. World J.*, 2014, **2014**, 128414.
6 Q. Lin, A. Armin, R. C. R. Nagiri, P. L. Burn and P. Meredith, *Nat. Photonics*, 2015, **9**, 106–112.
7 K. Galkowski, A. Mitioglu, A. Miyata, P. Plochocka, O. Portugall, G. E. Eperon and J. T.-W. Wang, *Energy Environ. Sci.*, 2016, **9**, 962–970.
8 C. Bi, Y. Shao, Y. Yuan, Z. Xiao, C. Wang, Y. Gao and J. Huang, *J. Mater. Chem. A*, 2014, **2**, 18508–18514.
9 S. H. Chang, K.-F. Lin, H.-M. Cheng, C.-C. Chen, W.-T. Wu, W.-N. Chen, P.-J. Wu, S.-H. Chen and C.-G. Wu, *Sol. Energy Mater. Sol. Cells*, 2016, **145**, 375–381.
10 Z. Guo, J. S. Manser, Y. Wan, P. V. Kamat and L. Huang, *Nat. Commun.*, 2015, **6**, 7471.
11 G. Niu, W. Li, J. Li, X. Liang and L. Wang, *RSC Adv.*, 2017, **7**, 17473–17479.
12 M. Zhang, J. S. Yun, Q. Ma, J. Zheng, C. F. J. Lau, Z. Deng, J. Kim, D. Kim, J. Seidel, M. A. Green, S. Huang and A. W. Y. Ho-Baillie, *ACS Energy Lett.*, 2017, **2**, 438–444.
13 Y. Hu, E. M. Hutter, P. Rieder, I. Grill, J. Hanisch, M. F. Ayguler, A. G. Hufnagel, M. Handloser, T. Bein, A. Harschuh, K. Tvingstedt, V. G. Dyakonov, A. Baumann, T. J. Savenije and M. L. Petrus, *Adv. Energy Mater.*, 2018, **8**, 1703057.
14 S. Kim, S. Bae, S.-W. Lee, K. Cho, K. D. Lee, H. Kim, S. Park, G. Kwon, S.-W. Ahn, H.-M. Lee, Y. Kang, H.-S. Lee and D. Kim, *Sci. Rep.*, 2017, **7**, 1200.
15 Y.-D. Lin, B.-Y. Ke, K.-M. Lee, S. H. Chang, K.-H. Wang, S.-H. Huang, C.-G. Wu, P.-T. Chou, S. Jhulki, J. N. Moorthy, Y. J. Chang, K.-L. Liau, H.-C. Chung, C.-Y. Liu, S.-S. Sun and T.-J. Chow, *ChemSusChem*, 2016, **9**, 274–279.
16 D. Bi, B. Xu, P. Gao, L. Sun, M. Grätzel and A. Hagfeldt, *Nano Energy*, 2016, **23**, 138–144.
17 F. Zhang, X. Liu, C. Yi, D. Bi, J. Luo, S. Wang, X. Li, Y. Xiao, S. M. Zakeeruddin and M. Grätzel, *ChemSusChem*, 2016, **9**, 2578–2585.
18 P. Agarwala and D. Kabra, *J. Mater. Chem. A*, 2017, **5**, 1348–1373.
19 L. Lei, S. Zhang, S. Yang, X. Li, Y. Yu, Q. Wei, Z. Ni and M. Li, *Nanotechnology*, 2018, **29**, 255201.
20 N. J. Jeon, J. H. Noh, Y. C. Kim, W. S. Yang, S. Ryu and S. I. Seok, *Nat. Mater.*, 2014, **13**, 897–903.
21 M. Xiao, F. Huang, W. Huang, Y. Dkhissi, Y. Zhu, J. Etheridge, A. Gray-Weale, U. Bach, Y.-B. Cheng and L. Spiccia, *Angew. Chem.*, 2014, **126**, 10056–10061.
22 K.-F. Lin, S. H. Chang, K.-H. Wang, H.-M. Cheng, K. Y. Chiu, K.-M. Lee, S.-H. Chen and C.-G. Wu, *Sol. Energy Mater. Sol. Cells*, 2015, **141**, 309–314.
23 C.-C. Chen, S. H. Chang, L.-C. Chen, C.-L. Tsai, H.-M. Cheng, W.-C. Huang, W.-N. Chen, Y.-C. Lu, Z.-L. Tseng, K. Y. Chiu, S.-H. Chen and C.-G. Wu, *Sol. Energy Mater. Sol. Cells*, 2017, **159**, 583–589.
24 S. H. Chang, W.-C. Huang, C.-C. Chen, S.-H. Chen and C.-G. Wu, *Appl. Surf. Sci.*, 2018, **445**, 24–29.
25 B. Cai, Y. Xing, Z. Yang, W.-H. Zhang and J. Qiu, *Energy Environ. Sci.*, 2013, **6**, 1480–1485.
26 M. Y. Ameen, S. Pradhan, M. R. Suresh and V. S. Reddy, *Opt. Mater.*, 2015, **39**, 134–139.
27 Y. Kato, L. K. Ono, M. V. Lee, S. Wang, S. Raga and Y. Qi, *Adv. Mater. Interfaces*, 2015, **2**, 1500195.
28 S. H. Chang, C.-C. Chen, L.-C. Chen, C.-L. Tien, H.-M. Cheng, W.-C. Huang, H.-Y. Lin, S.-H. Chen and C.-G. Wu, *Sol. Energy Mater. Sol. Cells*, 2017, **169**, 40–46.
29 Q. Chen, H. Zhou, T.-B. Song, S. Luo, Z. Hong, H.-S. Duan, L. Dou, Y. Liu and Y. Yang, *Nano Lett.*, 2014, **14**, 4158–4163.

